Low Grade Heat Driven Adsorption System For Cooling and Power Generation Using Advanced Adsorbent Materials

Al-Mousawi, Fadhel; Al-Dadah, Raya; Mahmoud, Saad

DOI:
10.1016/j.enconman.2016.08.012

Document Version
Peer reviewed version

Citation for published version (Harvard):
Al-Mousawi, F, Al-Dadah, R & Mahmoud, S 2016, 'Low Grade Heat Driven Adsorption System For Cooling and Power Generation Using Advanced Adsorbent Materials', Energy Conversion and Management, vol. 126, pp. 373-384. https://doi.org/10.1016/j.enconman.2016.08.012

Numerical Investigation of Effect of Fill Ratio and Inclination angle on a Thermosiphon Heat Pipe Thermal Performance

Ahmed. A. Alammar [a b *], Raya K. Al-Dadah [a], Saad M. Mahmoud [a]

[a] Department of Mechanical Engineering, University of Birmingham, Birmingham, United Kingdom

[b] Training and Development Centre, Ministry of Electricity, Baghdad, Iraq

* Email: Ghulfus_eng@yahoo.com; Mobile No: +447587832235

Abstract

Computational Fluid Dynamic (CFD) modelling of a heat pipe is a powerful tool that can be used to investigate the complex physical phenomena of the evaporation and condensation phase change processes inside thermosiphon heat pipes. In this work, a new CFD simulation of two phase flow inside thermosiphon heat pipe is carried out to investigate the effect of fill ratio (ratio of liquid volume to the evaporator volume) and inclination angle on its thermal performance in terms of temperature distribution and thermal resistance using FLUENT (ANSYS 15). Results of the CFD simulation were compared to published experimental data showing good agreement with maximum deviation of 4.2% and 8.1% for temperature distribution and thermal resistance, respectively. In addition, numerical results of inclination angle were also compared with experimental data in terms of thermal resistance giving maximum deviation of 1.3%. Using the validated CFD modelling, results showed that at low fill ratio and low inclination angle, there was a significant increase in the evaporator temperature. Regarding the thermal resistance, a fill ratio of 65% and inclination angle of 90^{o} produced the lowest thermal resistance for all the heat input values used. Also, as heat input increases, the effect of the fill ratio and inclination angle becomes more significant.

Keywords: CFD simulation, Ansys fluent, two phase closed thermosiphon, fill ratio, Inclination angle

NUMECLETURE

C_p	Specific heat	J/kg K	t	Time	s
D	Outside diameter of thermosiphon	m	u	Velocity	m/s
E	Total energy per unit mass	J/kg	***Greek symbols***		
F_S	Continuum surface force	Kg/m^2s^2	α	Volume fraction	
g	Acceleration gravity	m/s^2	μ	Dynamic viscosity	Pa s
h	Heat transfer coefficient	W/m^2 K	ρ	Density	Kg/m^3
h_{fq}	Latent heat	J/kg	σ	Surface tension coefficient	N/m
L	Height	m	***Subscripts***		
K	Thermal conductivity	W/m K	*con*	Condenser	
K_C	Surface curvature		*conv*	Convection	
P	Pressure	Pa	*cw,av*	Condenser wall, average	
Q_{con}	heat removed from condenser	W	*l*	Liquid	
S_q	Energy source term	J/m^3s	*mix*	Mixture	
S_{am}	Mass source term	Kg/m^3s	*Sat*	Saturation	
T	Temperature	K	*v*	Vapour	

1. Introduction

Heat pipes are devices for transferring heat from one point to another by evaporating and condensing the working fluid in a sealed vessel. They have the advantages of low thermal resistance, compact and uses small amount of working fluid thus are used in wide range of applications such as electronics cooling, heat exchangers and solar collectors. The main sections in the heat pipe are evaporator and condenser in which the heat is absorbed by working fluid in the evaporator side and rejected in the condenser. The vapour condensates by giving up its latent heat to the coolant at the condenser section and the condensate returns back to the evaporator by capillary force in the case of wicked heat pipe or by gravity in the case of wickless heat pipe (Thermosiphon). Considerable interest has been paid to wickless Two-Phase Closed Thermosiphon (TPCT) heat pipes due to their simple construction and low cost [1-3].

Although many experimental studies have been performed to examine the impact of working fluid fill ratio and inclination angle on the performance of different types of heat pipes, limited number of these studies have tested the performance of two phase closed thermosiphon. Noie [4] studied the effect of

filling ratio and the evaporator aspect ratio (evaporator length to evaporator diameter) on the heat transfer performance of the TPCT for a range of heat input. It was found that changing the fill ratio can reduce the evaporator wall temperature depending on the aspect ratio. Jiao et al [5] developed an analytical model to investigate the effect of filling ratio on the steady state heat transfer characteristics of a vertical wickless heat pipe and compared the results with their experimental work. They reported that the fill ratio depends on geometrical parameters and heat input. Jouhara and Robinson [6] investigated experimentally the effect of using different working fluids namely, water, FC-84 and FC-3283 and two filling ratios (100% and 50%) on the performance of thermosiphon heat pipe. A small size thermosiphon of 10 W with different working fluids (water, methanol and acetone) and liquid fill at various input energy has been investigated by Mozumder et al [7]. The study showed that the effect of charging liquid can be indicated by temperature difference, thermal resistance and overall heat transfer coefficient. The influence of the charged liquid and adiabatic length on the thermal performance of a long heat pipe charged with R-134a has been examined by Sukchana and Jaiboonma, 2013 [8] who concluded that the optimum liquid charge and heat flux suitable for shorter adiabatic section were 15 % and 5.92 kW/m^2, respectively. Chehade et al [9] tested effects of fill ratio, inlet cooling water temperature and mass flow rate in condenser jacket on the performance of the two-phase closed loop Thermosiphon. They concluded that the best fill charge ratio is between 7% and 10% and the fastest start up occurs by using the optimal fill ratio.

An experimental study has been performed by Manimaran et al [10] to examine the effect of heat input, charge fill ratio, and angle of inclination on thermal characteristics of a heat pipe, who reported that the lower thermal resistance was obtained at fill ratio 75% and vertical orientation. Sadeghinezhad et al and Ghanbarpour et al [11, 12] investigated the effect of different nanofluids and inclination angle on the thermal characteristics of a sintered wick and screen mesh heat pipe, respectively. They reported that the orientation has a strong effect on the thermal performance of a heat pipe and the lower thermal

resistance is obtained at an angle of 60^{o}. The effect of inclination angles on thermal performance of ammonia pulsating heat pipe and copper nanofluid heat pipe has been performed by Xue Zhihu and Qu Wei, and Senthilkurmar et al [13, 14], respectively. They demonstrated that the thermal performance of studied heat pipes increases as the inclination angle increases. Nazarimanesh et al [15] performed an experimental study to investigate the thermal of performance sintered heat pipe at various degree of inclination. They found that the lowest thermal resistance for base working fluid is achieved at an angle of 90^{o}.

There have been limited published CFD research work conducted to analyse TPCT heat pipes despite their numerous applications [16]. Fadhl et al [16] developed a CFD model to simulate condensation and evaporation processes inside the TPCT. CFD results were compared with experimental data in terms of temperature distribution along the heat pipe and thermal resistance at different heat inputs. They reported that the thermal performance of thermosiphon heat pipe improved by increasing heat input over 172 W.

Alizadhdakel et al [17] have reported experimentally the effect of input energy and fill ratio on the performance of a wickless heat pipe. They have also carried out a CFD simulation to investigate the phase change phenomena with effect of noncondensable gases throughout thermosiphon, and compered the results of experiment and CFD model. An optimum value for fill ratio of 50% was concluded for the studied thermosiphon and heat input range. A three dimension CFD analyses to investigate the effect of water with different concentrations of nanoparticles on the thermosiphon heat pipe performance has been performed by Humic and Humic [18]. Results showed that the concentration of nanoparticles in water had a considerable effect on the heat transfer characteristics of The TPCT. Fadhl et al [19] carried out a CFD simulation of a wickless heat pipe with R134a and R404a as working fluids, and Results were compared with published experimental data in terms of temperature distribution along the wall of TPCT. They found that thermal characteristics of both fluids inside the

thermosiphon differ significantly from that of water. A numerical CFD analysis and experimental work to investigate cooling water flow rate, input energy an orientation on the thermal performance of a thermosiphon heat pipe have been carried out by Abdullahi [20]. Results show that the heat transfer characteristics of the TPCT increase as inclination angle and input energy increase. Kim et al [21] implemented a CFD simulation to study the effect of the condensation frequency on the mass transfer rate during phase change inside a thermosiphon heat pipe. The study concluded that the condensation frequency should be considered as $0.1\times(\rho_l/\rho_v)$ to accurately simulate the mass transfer process during condensation and evaporation phenomena.

From all mentioned experimental investigations, it can be concluded that the best fill ratio and inclination angle for any heat pipe depend on many factors such as geometry, heat input, type of liquid and operating conditions. Therefore, according to these parameters, the suitable inclination angle and liquid charge ratio change from one heat pipe to another and investigations to identify the best fill ratio and inclination angle is needed whenever anyone of these parameters is changed. For that reason, a numerical study should be used to specify optimum charging ratio and orientation before the experimental work to reduce time and cost of these investigations. In addition, all stated numerical CFD studies were not employed to analyse these effects. Thus, in the present study, a new CFD model was developed to investigate the influence of five different values of fill ratio (25%, 35%, 65%, 80% and 100%) of water and inclination angle range of (10, 30, 50, 70, and 90^o) on the thermal performance of a two-phase closed thermosiphon at various values of heat input. Consequently, wide range of affecting parameters can be modelled to investigate their effect on the performance of the heat pipe.

2. GOVERNING EQUATIONS

Many researchers have used Volume of Fluid (VOF) model to solve numerically a multiphase flow because it is easier compared with finite volume method. Reasons behind that are that the location of

the interface between phases varies for each computational step, and physical properties at the interface are also changeable which make the numerical simulation computationally expensive. Thus, solving these problems can be achieved using VOF model by defining the motion of all phases and tracking the location of the interface accordingly [16-28]. In the VOF model, movement of different fluids can be tracked by solving a single set of Navier-Stocks equations for the volume fraction of each fluid throughout the computational cell [28]. Therefore, the existence of a certain phase in any control volume can be easily specified from the volume fraction according to the following three cases:

α_l= 1: The cell is full of vapour

α_v = 0: The cell is full of liquid

$0 < \alpha_v < 1$: The cell contains a mixture of liquid and vapour

The third case means

$$\alpha_l + \alpha_v = 1 \qquad [1]$$

Where α_l and α_v are volume fractions of liquid and vapour respectively.

In order to define the motion of the fluid inside the TPCT during evaporation and condensation processes, the governing equations of mass continuity, momentum and energy with source terms are solved using Fluent Ansys.

2.1 Continuity Equation

$$\frac{\partial}{\partial u}(\rho) + \nabla \cdot (\rho \vec{u}) = 0 \qquad [2]$$

Where, ρ and u are the density and velocity of the fluid.

To track the interface between phases, solution of eq. (2) for the volume fraction is needed. Therefore, for the secondary phase (liquid phase) of VOF model, this equation can be written as follow:

$$\frac{\partial}{\partial u}(\alpha_l \rho_l) + \nabla \cdot (\alpha_l \rho_l \vec{u}) = S_{\alpha m} \quad [3]$$

Where, $S_{\alpha m}$ is the mass source term that can be used to find the mass transport from one phase to another during the evaporation and condensation processes. The above equation solves for the secondary phase (l) only and the volume fraction for the primary phase (v) can be calculated using eq. (4):

$$\sum_{k=1}^{2} \alpha_k = 1 \quad [4]$$

2.2 Momentum Equation

$$\frac{\partial}{\partial u}(\rho \vec{u}) + \nabla \cdot (\rho \vec{u}\vec{u}) = -\nabla p + \rho \vec{g} + \nabla . \left[\mu (\nabla \vec{u} + \nabla \vec{u}^T) - \frac{2}{3} \mu \nabla . uI \right] + F_S \quad [5]$$

Where, the fluid properties ρ and μ are expressed by eq. (6) and eq.(7) respectively. According to the VOF model, the physical properties are determined for the mixture only based on the value of volume fractions of liquid and vapour.

$$\rho = \alpha_l \rho_l + \alpha_v \rho_v \quad [6]$$

$$\mu = \alpha_l \mu_l + \alpha_v \mu_v \quad [7]$$

F_S is the Continuum Surface Force (CSF) acting on the interface between two phases which was proposed by Brackbill [29] and is used in Fluent Ansys to include the effect of surface tension. This term can be expressed as follow [30]:

$$F_S = 2\sigma \frac{\alpha_l \rho_l k c_v \nabla \alpha_v + \alpha_v \rho_v k c_l \nabla \alpha_l}{\rho_l + \rho_v} \quad [8]$$

Where, σ is the interfacial tension between two phases, Kc_l and Kc_v are surface curvatures of liquid and vapour respectively that can be written in the following forms:

$$kc_l = \frac{\Delta\alpha_l}{|\nabla\alpha_l|} \quad [9], \qquad kc_v = \frac{\Delta\alpha_v}{|\nabla\alpha_v|} \quad [10]$$

2.3 Energy Equation:

$$\frac{\partial}{\partial u}(\rho E) + \nabla\cdot[\vec{u}(\rho E + p)] = -\nabla.(k\nabla T) + S_q \quad [11]$$

Where, *E* and *K* are the internal energy and thermal conductivity which can be computed from Eq. (12) and Eq. (13) respectively, again, for mixture only.

$$k = \alpha_l k_l + \alpha_v k_v \quad [12]$$

$$E = \frac{\alpha_l \rho_l Cp_l + \alpha_v \rho_v Cp_v}{\alpha_l \rho_l + \alpha_v \rho_v}(T - T_{sat}) \quad [13]$$

Where, k_l and k_v are the thermal conductivity of liquid and vapour and Cp_l and Cp_v are the specific heat of liquid and vapour respectively. S_q, is the energy source term which can be employed to determine the heat transfer during the phase change which is calculated from mass source term $S_{\alpha m}$ and the latent heat (h_{fg}) as follow:

$$S_q = S_{\alpha m} h_{fg} \quad [14]$$

Single momentum equation and energy equation will be solved all over the control volume for both fluids. Accordingly, the computed velocity and temperature will be shared between two phases.

2.4 Phase Change Equations

In order to model the transport phenomenon inside the thermosiphon represented by mass and heat transfer from one phase to another during evaporation and condensation processes, source terms proposed by De Schepper et al [22] need to be added to the continuity and energy equations used by the

VOF model in Fluent Ansys. As stated previously, a single volume fraction equation will be solved for each cell for secondary phase while the volume fraction for the primary phase will be obtained from eq.(4). Therefore, to describe the mass transfer related to the evaporation process, two equations are needed, one for liquid phase and another for vapour phase as follow:

Evaporation $T_{mix} > T_{sat}$

Liquid phase:

$$S_{\alpha M} = -0.1\alpha_l \rho_l \left| \frac{T_{mix} - T_{sat}}{T_{sat}} \right| \quad [15]$$

Vapour phase:

$$S_{\alpha M} = 0.1\alpha_l \rho_l \left| \frac{T_{mix} - T_{sat}}{T_{sat}} \right| \quad [16]$$

Similar to the evaporation process, two expressions are also required to represent the mass transfer during the condensation process. Again, one for liquid and another for vapour as follow:

Condensation $T_{mix} < T_{sat}$

Liquide phase:

$$S_{\alpha M} = 0.1\alpha_v \rho_v \left| \frac{T_{mix} - T_{sat}}{T_{sat}} \right| \quad [17]$$

Vapour phase:

$$S_{\alpha M} = -0.1\alpha_v \rho_v \left| \frac{T_{mix} - T_{sat}}{T_{sat}} \right| \quad [18]$$

Accordingly, the energy source term S_q that needs to be added to the energy equation (eq. (11)) to represent the amount of heat transfer from one phase to another during the evaporation and condensation processes can be determined from eq. (14) as follow:

Evaporation

$$S_q = -0.1\alpha_l \rho_l \left| \frac{T_{mix} - T_{sat}}{T_{sat}} \right| h_{fg} \quad [19]$$

Condensation

$$S_q = 0.1\alpha_v \rho_v \left| \frac{T_{mix} - T_{sat}}{T_{sat}} \right| h_{fg} \quad [20]$$

Where, T_{mix} and T_{sat} are the temperature of mixture and saturation temperature respectively. Equations (15-20) are set in a sub-program and linked to the Fluent to add the calculated mass source terms (eqs.15-18) and energy source terms (eqs.19 and 20) to the mass conservation equation (3) and energy equation (11) respectively in the VOF model in order to completely model the phase change process.

3. CFD SIMULATION SET UP

3.1 Geometry and Mesh

Geometry of a vertical two-dimension wickless heat pipe has been generated using workbench design modular (Ansys 15). The geometry represents a copper tube with a total height of 400 mm, outer and inner diameters of 22 and 20.2 mm respectively. The thermosiphon is divided into two sections, evaporator and condenser with height of 200 mm each as illustrated in Fig. 1. These dimensions are chosen to be similar to geometry of a previous experimental work by Abdullahi [20] to validate the CFD simulation.

Workbench design modular (Ansys 15) was also used to mesh the geometry where Control edge sizing technique was employed to control the grid in every domain and to govern cell sizes near inner walls and inside the solid domain (walls) with bias factor of 10 used in these regions to ensure that the flow and heat transfer can be correctly captured in these areas. The number of cells in the fluid domain was 24522 and 9620 grids in the solid domain. The mesh size and type are shown in Fig. 2.a.

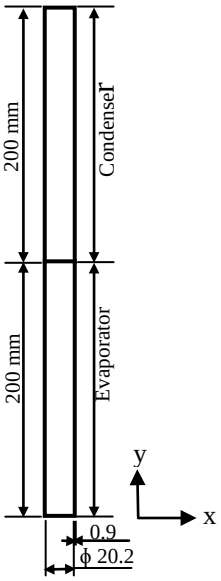

Fig.1. Heat pipe geometry

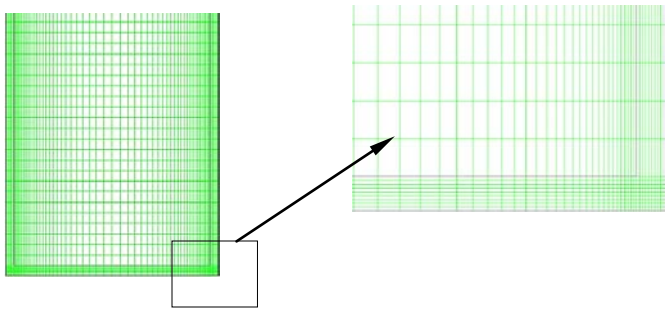

Fig.2.a. Mesh of zoomed section

3.2 Initial and Boundary Conditions

Five different filling ratios and inclination angles are used in this study namely, 25%, 35%, 65%, 80% and 100% of the evaporator volume, and 10, 30, 50, 70 and 90^{o}, respectively. To set up the fill ratio for each case, the corresponding evaporator height is initially patched with liquid while the remaining height is patched with vapour. In addition, the inclination angle is defined as the inclination of thermosiphon from the horizontal axis and can be set up by multiplying y-component of acceleration gravity with sine of the angle and x-component with cosine as shown in fig.2.b.

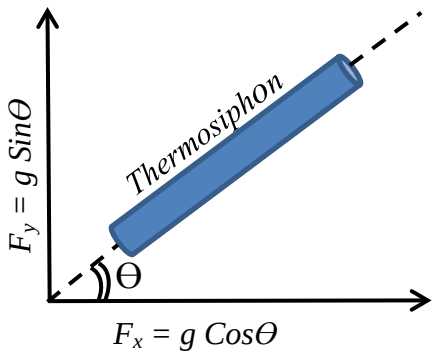

Fig.2.b. Inclination angle of thermosiphon heat pipe

The initial temperature of both evaporator wall and liquid should be selected slightly above the boiling point which was chosen to be 373 ^{o}K to insure that the boiling process occurs once simulation time starts to reduce computational time [30] and the condenser wall and fluid temperatures were set as 290 ^{o}K (condenser cooling temperature). Operating temperature should be set to be the smallest temperature in the system (290 ^{o}K) and operating density must be set as 0 Kg/m^3 when ideal gas is used and as the smallest density in the system when constant gas density is used [30]. In addition, saturation temperature and operating pressure were set to be 373 ^{o}K and 101325 Pa, respectively.

At the internal walls of evaporator and condenser sections, a non-slip boundary condition is applied, while a constant heat flux is imposed at the outer wall of the evaporator to simulate the heat added to the thermosiphon. Three values of heat flux were employed 2858, 5910 and 7346 W/m^2 corresponding to heat transfer rates 39, 81 and 101W respectively, which is taken from [20]. The top and the bottom ends of the thermosiphon is assumed to be insulated, which means no cooling or heating effect applied at these walls. As a result, a zero heat flux is defined at these ends. To model the heat removed from the condenser section, a convection boundary condition is applied at the outer wall of the condenser section. Thus, the heat transfer coefficient between cooling water and the condenser's wall needs to be calculated from the following relation:

$$h_{conv} = \frac{Q_{cond}}{2\pi D L_{cond} (T_{cw,av} - T_m)} \qquad [21]$$

Where, h_{conv} is the convection heat transfer coefficient between the cooling water and the condenser's wall, Q_{cond} is the heat removed from the condenser section, $T_{cw,av}$ is the average wall temperature of the condenser section and T_m is the mean temperature of the cooling water. Values of Q_{cond}, and T_m are obtained from Abdallahi [20] experimental work.

To include the effect of the interfacial force between liquid and vapour, the term F_s is added to the momentum equation eq. (5) by activating the CSF in the fluent. Consequently, the value of the surface tension in eq. (6) can be computed from the following formula [16]:

$$\sigma = 0.09805856 - 1.845 \times 10^{-5} T - 2.3 \times 10^{-7} T^2 \quad [22]$$

3.3 Solution Methods and Techniques

In present analysis, the VOF model is used to simulate the multi-phase flow, while the gravitational acceleration of 9.81 m/s^2 is activated to include a body force term. The water liquid is chosen to be a secondary phase (liquid phase) and its density can be determined from the following relation [16]:

$$\rho_l = 859.0083 + 1.252209T - 0.0026429T^2 \quad [23]$$

A transient solution with a time step of 0.001s is employed for all cases due to dynamic behaviour of the two-phase flow [17, 22]. A combination of the SIMPLE algorithm for pressure-velocity coupling and first-order upwind scheme for the calculation of the momentum and energy are used. For determination of the volume fraction and pressure, Geo-Reconstruct and PRESTO discretisation are chosen, respectively [16, 17]. The solution is considered to be converged when the residuals of the mass and velocity components are reduced to 10^{-4} while the residuals of the temperature variables are reduced to 10^{-6}.

4. RESULTS AND DISCUSSION

4.1 Validation of the CFD Solution

To validate the CFD simulation, same geometry and boundary conditions as Abdullahi [20] have been adopted. Therefore, the temperature distribution along the wall and the thermal resistance of the thermosiphon for the stated three different heat inputs which are determined from CFD modelling have been compared with those obtained from Abdullahi [20] experimental work.

A comparison of the temperature distribution along thermosiphon wall between the CFD modelling (current work) and the experimental work [20] is illustrated in fig.3 for three input energies. It is shown that the CFD simulation (solid lines) predicts well the experimental results (marks). However, there is a slight deviation (maximum 4.2%) at the bottom of the evaporator and the top of the condenser where the difference becomes larger at larger heat input.

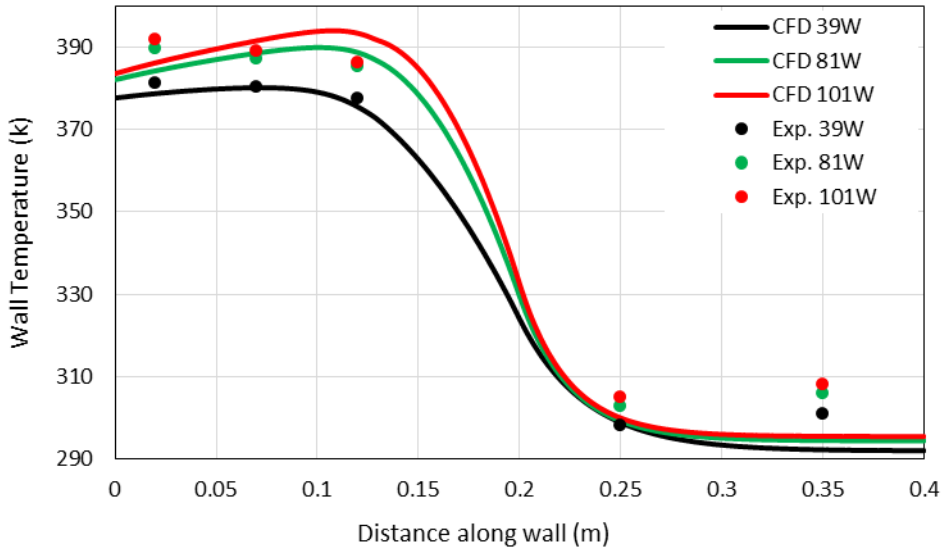

Fig.3. comparison of Variation of temperature along the wall of thermosiphon between experimental data and CFD results (Vertical orientation)

Figure (4) presents a comparison of the thermal resistance between CFD simulation and experimental study [20] at different heat inputs. It is observed that the CFD solution over predicts the experimental

results by 8.1%. This is due to higher evaporator temperature and lower condenser temperature obtained from the CFD solution, which yield higher thermal resistance. However, the same trend has been achieved in which the thermal resistance decreases with increasing the heat input.

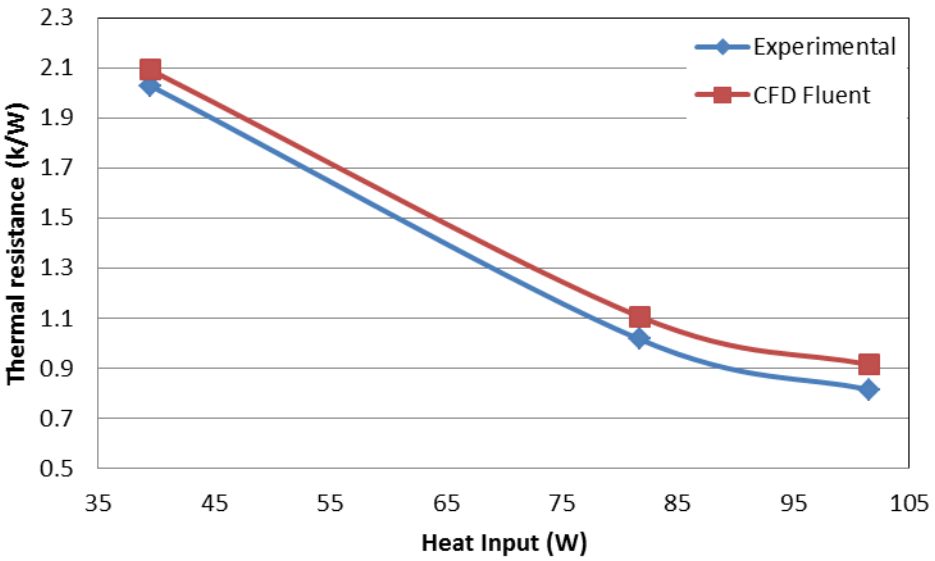

Fig.4. Comparison of Variation of the thermal resistance with heat input between experimental data and CFD results (Vertical orientation)

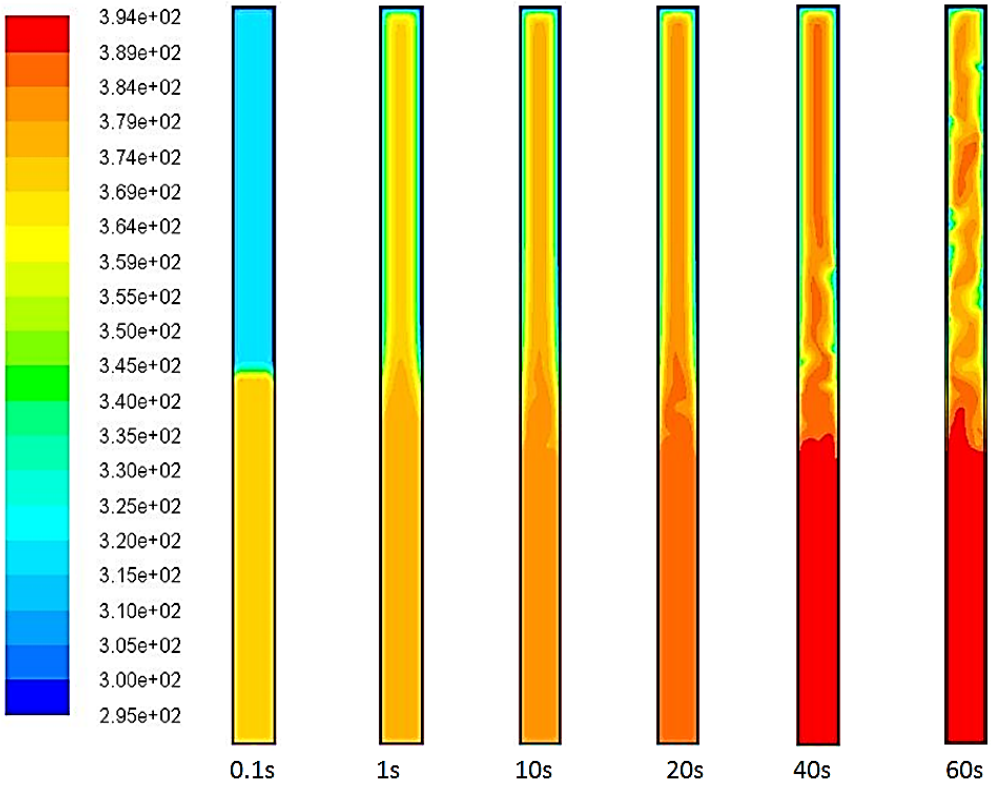

Fig.5.Temperature contours at various simulation times (101W, 65 % and 90^{o})

T Figure (5) shows the heat transfer process represented by temperature contours during simulation time at heat input 101W, fill ratio 65% and vertical orientation. Firstly, heat transfer from evaporator wall to the liquid due to constant heat flux, then, when the working fluid reaches its saturation temperature, it starts boiling and the phase change occurs. Therefore, vapour raises up to heat the upper part of the heat pipe and the temperature increases accordingly with time until reaching the steady state.

The variation of the vapour volume fraction with simulation time is illustrated in figure (6) in which the red colour refers to vapour phase (volume fraction=1) and the blue one refers to liquid phase (volume fraction=0). At the beginning, a very small bubble size is observed at time 0.1 second, then, bubbles size and number increase as simulation time increases due to increase in the temperature of the liquid reaching the boiling temperature and, hence, the steady state condition at time 60 seconds.

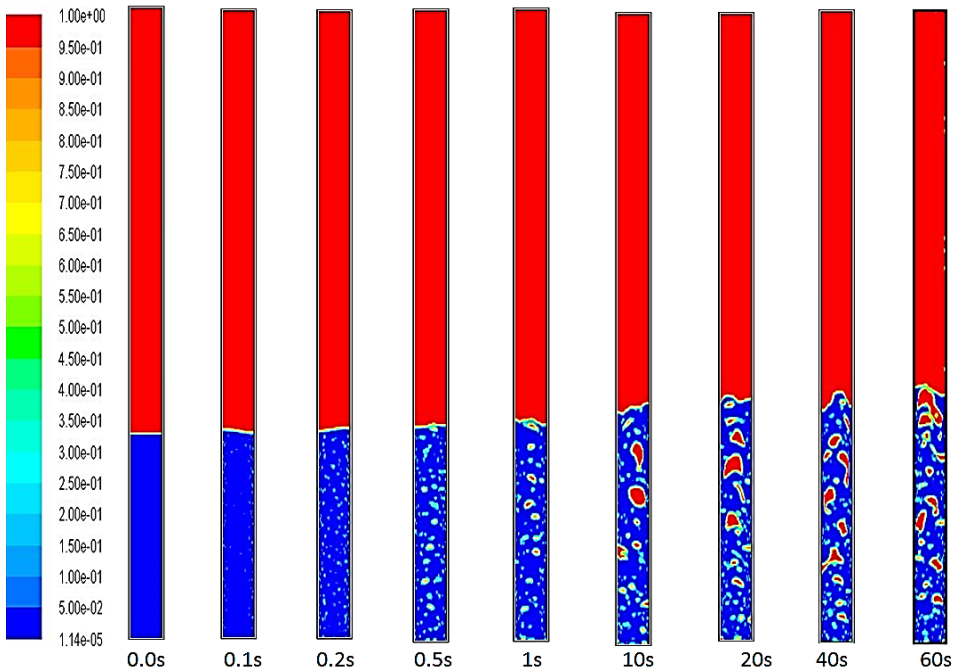

Fig.6.Vapour volume fraction contours at various simulation times (101W, 65 % and 90^{o})

4.2 Fill Ratio Effect

The influence of the volume of the charged liquid on the thermal performance of the (TPCT) is obtained by employing the CFD simulation. Therefore, the temperature distribution on the outer wall of the thermosiphon for fill ratios 25%, 35%, 65%, 80% and 100% is shown in figures (7.a), (7.b) and (7.c) at heat inputs of 39, 81 and 101W respectively. Figures (7.a, b and c) show similar trends in temperature distribution along the wall of thermosiphon at three heat inputs for each fill ratio. It is also observed that the effect of changing fill ratio and increasing heat input on temperature profile is more significant in the evaporator section than in condenser section. In addition, a lowest wall temperature distribution is seen at fill ratio 65% for all input energies. On the other hand, a high wall temperature occurs at the mid-distance of the evaporator wall at fill ratio 25% and 35% for all heat inputs. This wall temperature increases with increasing the heat input until reaching the highest value at heat input 101W and fill ratio 25%. For fill ratios 80% and 100%, a higher wall temperature in upper part of the evaporator is observed compared with other values of fill ratio for three heat inputs. This is due to higher liquid height in the evaporator which prevents large bubbles to reach liquid surface forming a vapour film on the inner wall of the evaporator and hence, increasing the wall evaporator temperature in that region. The effect of higher liquid height decreases with increasing the heat input in the case of 80% fill ratio whereas increases in the case of 100%.

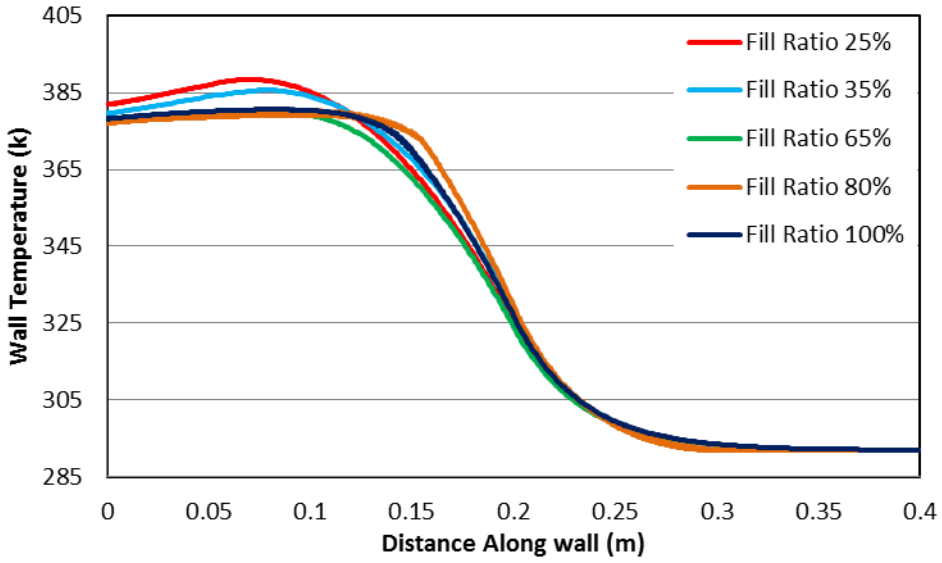

Fig.7.a Variation of temperature with the distance along the wall of the thermosiphon at heat input 39 W for different fill ratios (Vertical orientation)

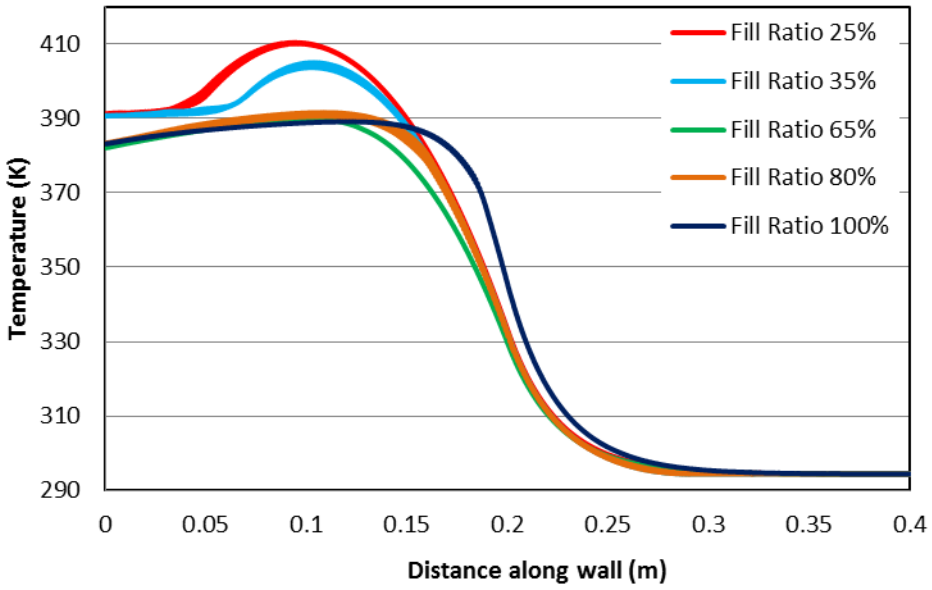

Fig.7.b Variation of temperature with the distance along the wall of the thermosiphon at heat input 81 W for different fill ratios (Vertical orientation)

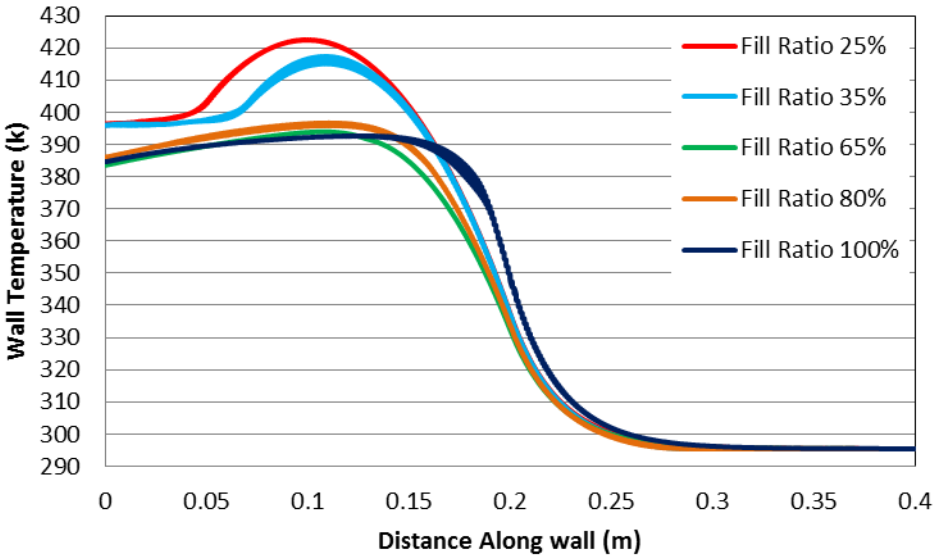

359

360 Fig.7.c Variation of temperature with the distance along the wall of the thermosiphon at heat input 101

361 W for different fill ratios (Vertical orientation)

362

363 Figure (8) presents the effect of the fill ratio on the average wall temperature of the evaporator for three

364 heat inputs. It is shown that the average evaporator wall temperature decreases from its maximum value

365 at fill ratio 25% to the minimum value at 65% then increases again to a certain value at fill ratios 80%

366 and 100% for input energies 81and 101W (similar trend was obtained by [9]). However, at heat input

367 39 W, there is a slight change in evaporator wall temperature between fill ratios 25% and 35% and after

368 fill ratio 80% the trend decreases slightly at fill ratio 100%. Therefore, the effect of fill ratio on

369 evaporator wall temperature is more clear at relatively high input energy (81and 101W) than that at low

370 energy (39W).

371

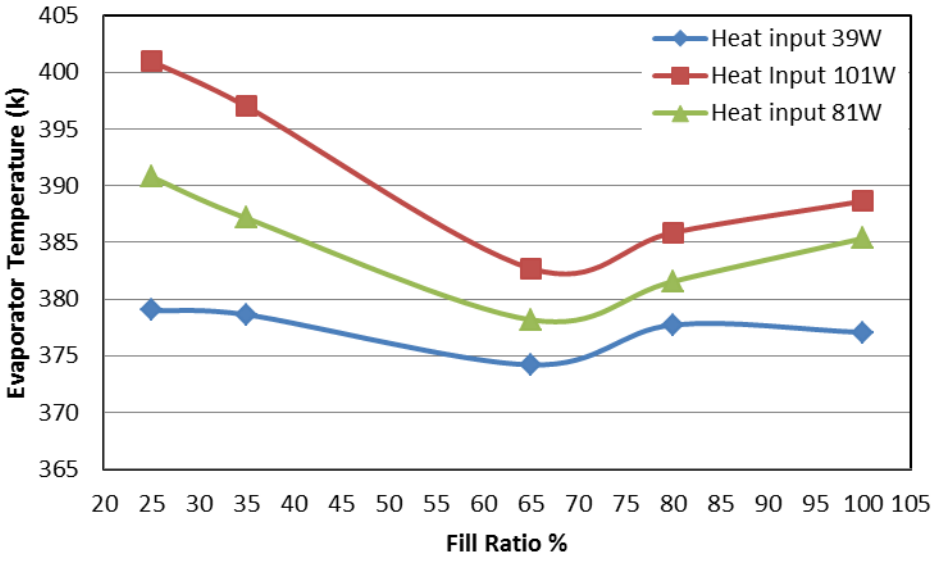

Fig.8. Variation of average wall temperature of evaporator with fill ratio at different heat inputs (Vertical orientation)

Figure (9) shows the effect of heat input on thermal resistance for various fill ratios. It is seen that the thermal resistance decreases with increasing heat input for all fill ratios. A higher thermal resistance is observed at fill ratio 25% due to a small amount of working fluid whereas a lower value at 65% for all energy inputs (similar trend was obtained by [10]). However, a lower difference in thermal resistance between the fill ratios is seen at heat input of (39W), especially, between 25% and 35% compared with that at higher energy inputs (81 and 101W). This indicates that with low fill ratios and a heat input of 101W, the heat pipe reaches its heat transfer limit leading to high temperatures at the upper part of the evaporator as shown in figures 7.b and 7.c. In addition, the thermal resistance for fill ratio 80% is greater than that for 100% at input energy 39W compared with that at higher heat inputs (81 and 101W). Thus, the best fill ratio is 65% and this is a similar conclusion as those were concluded by [17] and [10]. The reason behind increasing the evaporator wall temperature and, hence, the thermal resistance at high fill ratios (80% and 100%) attribute to the fact that the thermal resistance of liquid film in the evaporator increases as liquid height increase (fill ratio) above the optimum value.

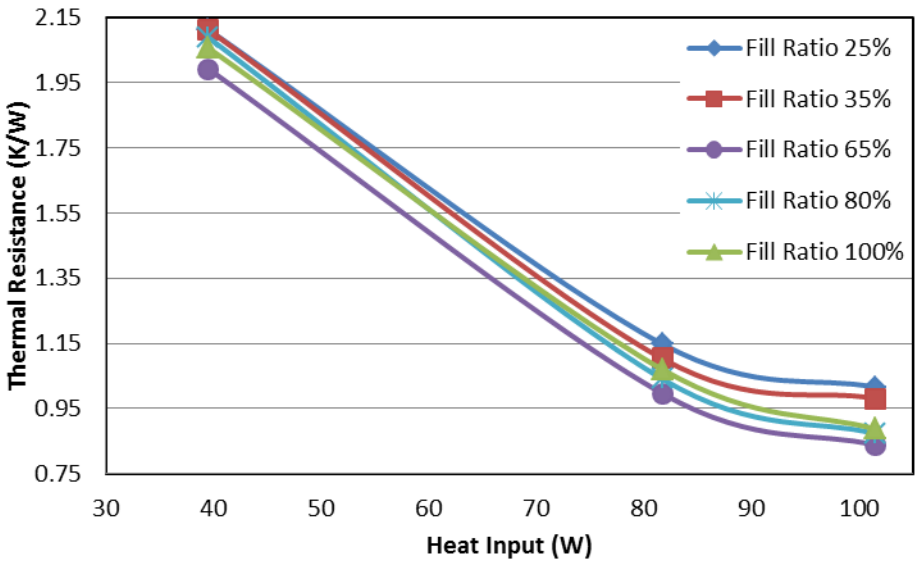

Fig.9. Variation of thermal resistance with heat inputs at different fill ratios (Vertical orientation)

4.3 Effect of Inclination Angle

CFD simulation has been used to investigate the effect of inclination angle on the thermal performance of the thermosiphon at angles of (10, 30, 50, 70 and 90^{o}). Firstly, the numerical results were compared with the experimental work of Abdullahi [20] in terms of thermal resistance to validate the CFD solution. Fig.10 presents a comparison of variation of thermal resistance with inclination angle of thermosiphon at heat input 109W between CFD modelling and experimental work [20]. CFD results show a good agreement with experimental data with maximum deviation of (1.3%) and produce a similar trend in which the lowest thermal resistance is obtained at angles of (80 and 90^{o}) whereas the highest at (70^{o}).

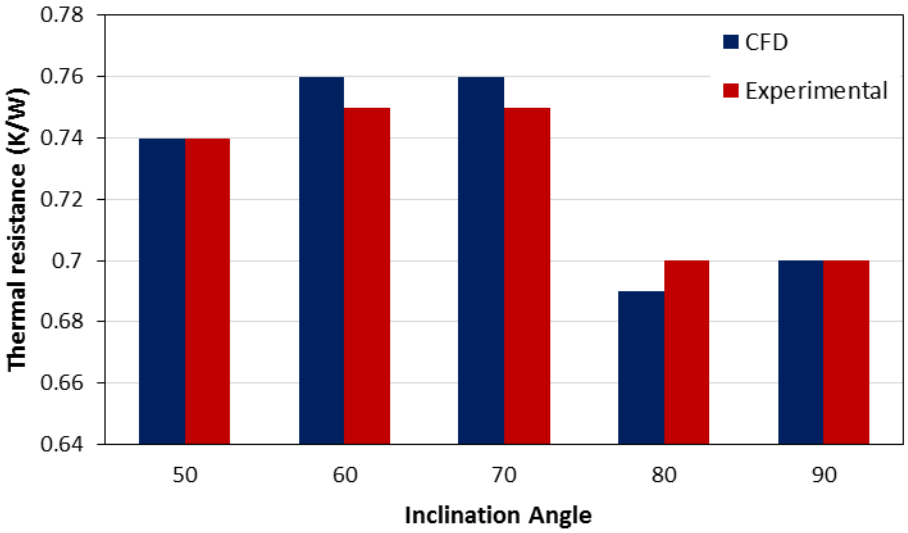

Fig.10. Comparison of variation of thermal resistance with inclination angle between CFD result and experimental work (109W and FR=65%)

Figure (11.a) presents the variation of vapour volume fraction during flow time for inclination angle of 10^{o}, heat input 101W and fill ratio 65%. It is clear that the liquid in evaporator is not in contact at certain parts of evaporator wall due to inclination leading to increase the wall evaporator temperature. In addition, it is observed that the bubble size remains relatively small as time increases and this may be attributed to the nearness of liquid surface to the bubble nucleation sites because of the inclination. As a result, a vapour film forms on the upper part of the evaporator wall which leads to additional increase in evaporator wall temperature. Fig.11.b shows the vapour volume fraction at simulation times 3 and 60 seconds for different fill ratios. Relatively small bubbles are observed for fill ratios 25% and 35% due to nearness of liquid surface from bubble sites. On the other hand, for fill ratios 80% and 100%, many large bubbles stuck on evaporator wall before they reach liquid surface due to high height of liquid column resulting in higher evaporator temperature compared with fill ratio 65%.

Bubble dynamics and frequency can be greatly changed by changing surface wettability in terms of contact angle [31]. This also depends on the type of fluid used where the contact angle is a function of

surface tension which changes from one fluid to another. Therefore, investigating of such point would be important to study the effect of these parameters on the thermal performance of thermosiphon heat pipe in future work.

.

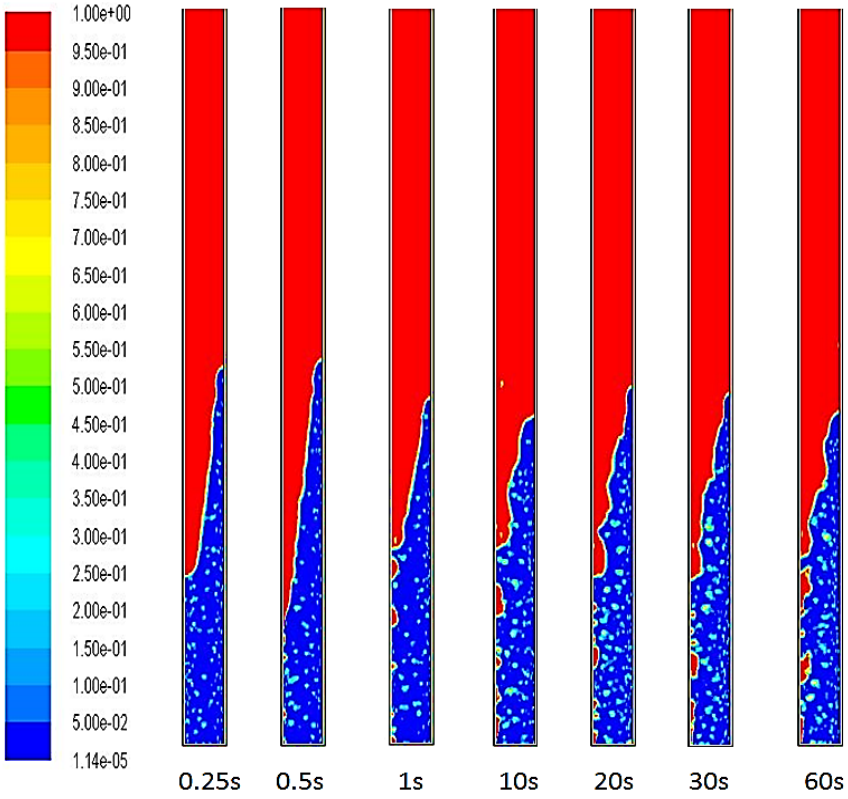

Fig.11.a. Vapour volume fraction contours at various simulation times for inclination angle 10^{o}

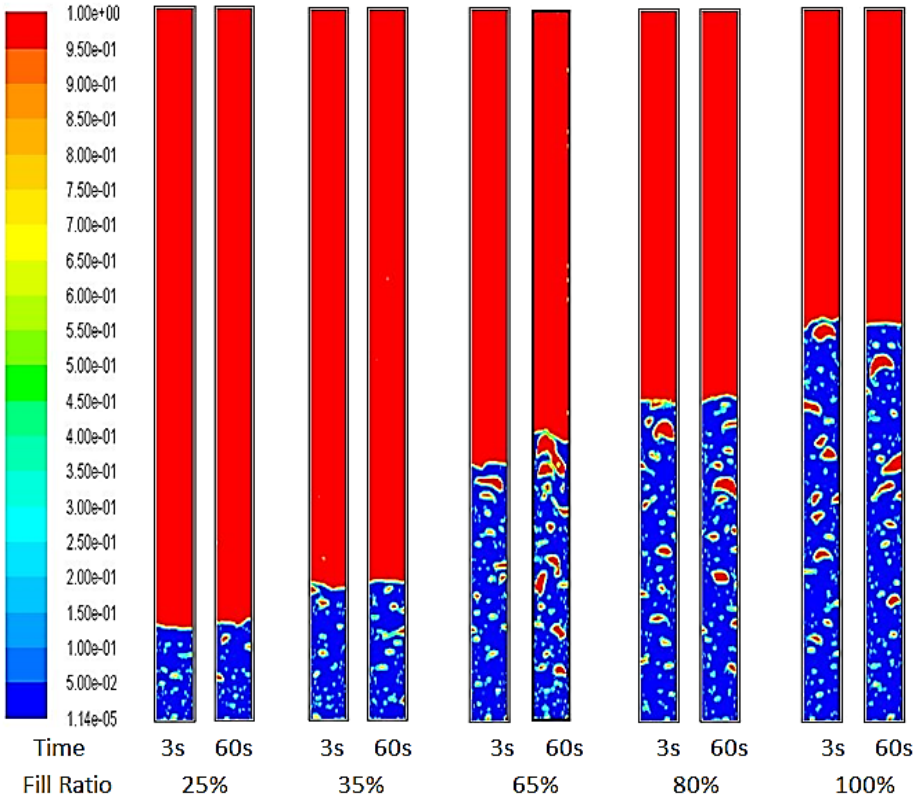

435

436 Fig.11.b. Vapour volume fraction contours at various simulation times for different fill ratios

437

438 Figures (12.a, 12.b and 12.c) illustrate the variation of the wall temperature of thermosiphon with the
439 distance along the wall for three heat inputs (39, 81 and 101W) at five inclination angles (10, 30, 50, 70
440 and 90) and fill ratio of 65%. They show a similar trend for three input energies in which the highest
441 and lowest wall temperature occur at angles of 10^{o} and 90^{o}, respectively. These higher temperatures at
442 low inclination angles attribute to the fact that some of the upper part of the evaporator section is not in
443 contact with liquid due to inclination. However, at the inclination angle of 10o and heat input 39 W, the
444 wall temperature near 0.2 m (at the beginning of the condenser section) remains constant for a short
445 distance and then decreases. This can be attributed to the existence of liquid at the lower part of the
446 condenser as a result of inclination near the horizontal orientation (10 degree) leading to blockage of
447 this part which prevents the temperature to decrease, after that, the wall temperature starts decreasing

again. This effect decreases as heat input increases (81W) due to increasing the evaporation rate which reduces the amount of liquid at that region allowing the wall temperature to decrease. It is also observed that the effect of inclination angle increases as the heat input increases.

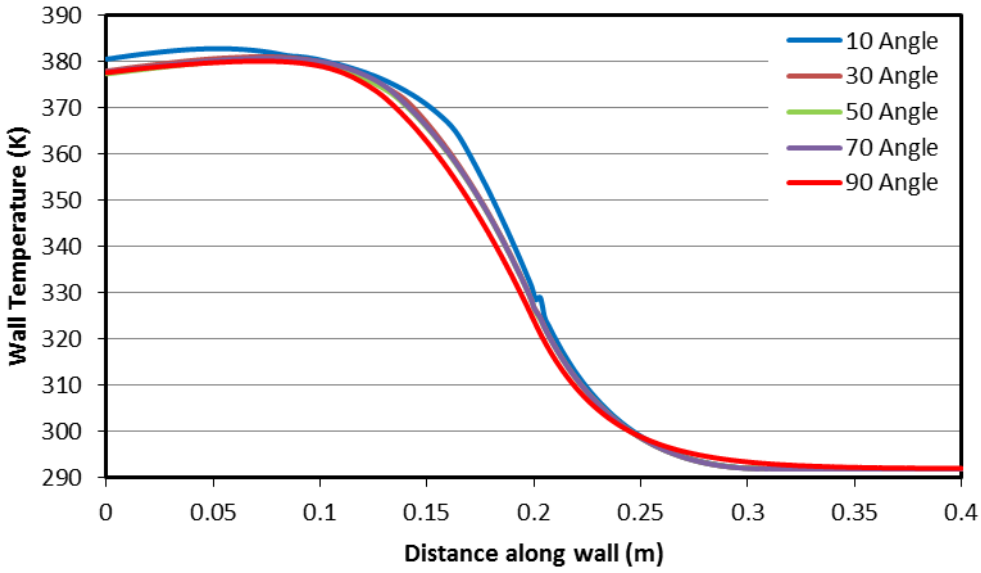

Fig.12.a. Wall temperature distribution at heat input 39W and fill ratio 65% for different inclination angles

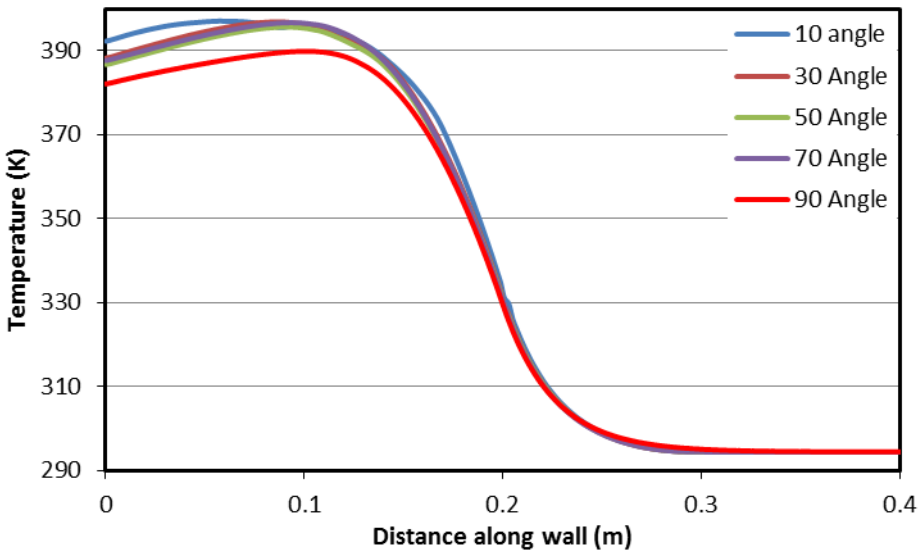

457

458

459 Fig.12.b. Wall temperature distribution at heat input 81W and fill ratio 65% for different inclination

460 angles

461

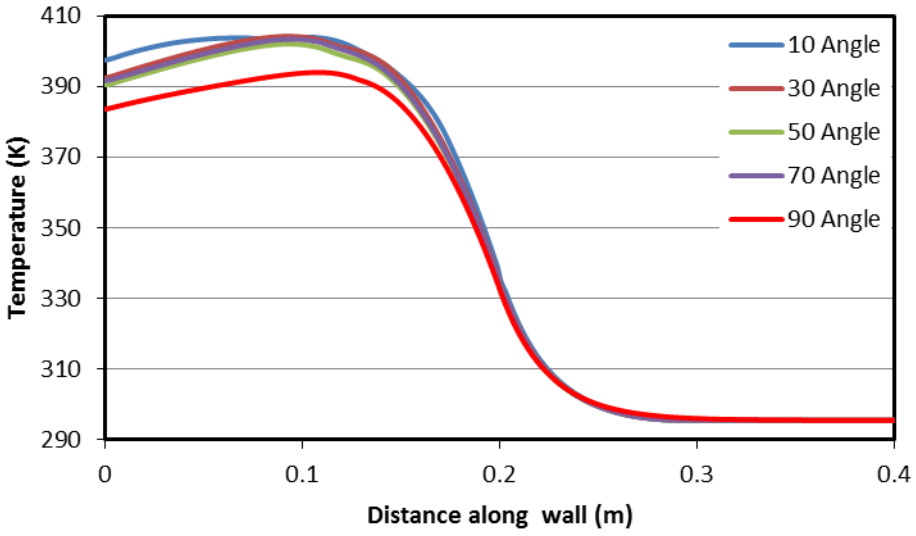

462

463 Fig.12.c. Wall temperature distribution at heat input 101W and fill ratio 65% for different inclination

464 angles

465

The effect of inclination angle on the average wall temperature of the evaporator at input energies of 39, 81, and 101W is illustrated in figure 13. It can be seen that the evaporator temperature increases as the inclination angle decrease toward the horizontal orientation for all heat inputs and this increase is higher when the heat input is higher. However, at angle of 50^{o} the value of the evaporator temperature is less than that at angle 70^{o} for all three cases, but it is still higher than the value at angle 90^{o}.

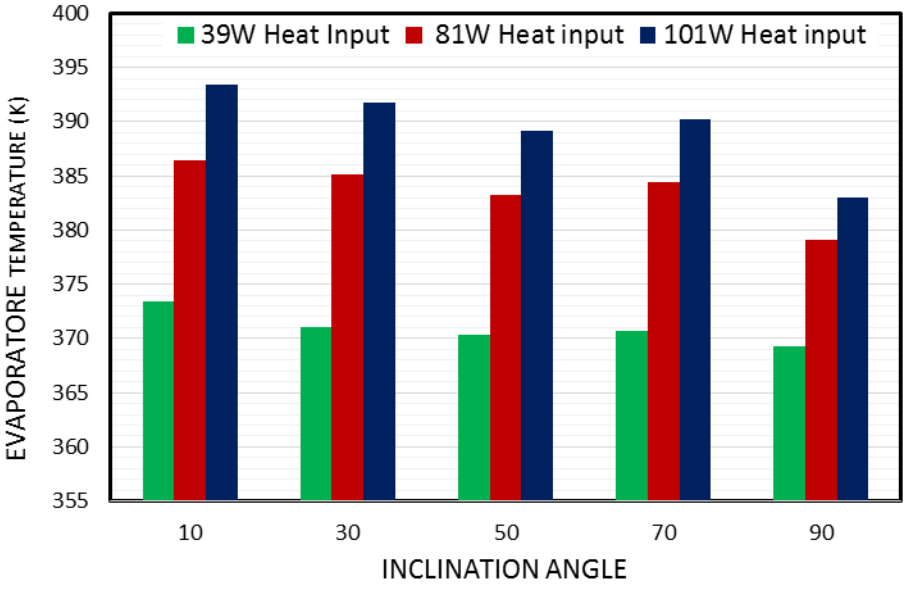

Fig.13. variation of the evaporator wall temperature with inclination angle at heat inputs 39, 81, and 101W (FR=65%)

Figure 14 shows the effect of inclination angle on the thermal resistance of the thermosiphon at heat inputs 39, 81, and 101W. The results show that the thermal resistance decreases as the inclination angle increases and the highest and lowest thermal resistance are at inclination angle 10^{o} and 90^{o}, respectively, for all input energies. Therefore, the thermal performance of the (TPCT) is better at vertical orientation (90^{o}) than that at other orientations (similar conclusions were reported by [10] and [15]).

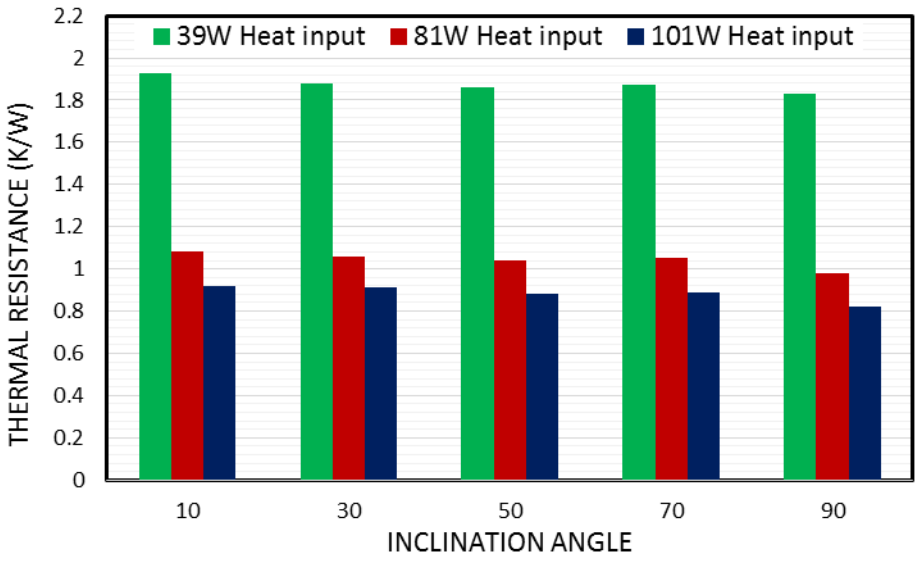

Fig.14. variation of the thermal resistance with inclination angle at heat inputs 39, 81, and 101W (FR= 65%)

5. CONCLUSIONS

The effect of five fill ratios of working fluid (25%, 35%, 65%, 80% and 100% of the evaporator volume) and five inclination angles (10, 30, 50, 70 and 90^{o}) on the performance of the tow phase closed thermosiphon was investigated numerically by developing a new CFD simulation. A comparison between the CFD solution and a published experimental work was also carried out for different heat inputs 39, 81 and 101W and at fill ratio of 65%. It is concluded that:

1- Developed CFD simulation was successfully used to model the TPCT and investigate the effect of fill ratio and inclination angle on its thermal performance. This proved by comparing the wall temperature distribution and thermal resistance for three input energies at fill ratio 65% with published experimental data, and maximum deviations of 4.2% and 8.1% has been reported, respectively. Regarding to inclination angle, a comparison in terms of thermal resistance for inclination angles of 50,

60, 70, 80 and 90^{o} at heat input 109W and fill ratio 65% has been carried out with a maximum deviation of 1.3%.

2- Heat transfer limit is reached when the volume of the charged liquid is small at fill charge ratio of 25% and 35%. This is observed when a considerable increase in evaporator wall temperature takes place, especially at higher energy input.

3- The lowest average evaporator wall temperature and thermal resistance take place at fill ratio of 65% and angle of 90^{o} whereas the highest at 25% and 10^{o} due to the effect of small fill ratio and inclination, respectively. This effect is higher as heat input increases.

4- The best fill ratio and inclination angle regarding to the thermal performance for this case were found to be 65% and 90^{o}, respectively.

Acknowledgement

The first author would like to acknowledge the Iraqi Ministry of Higher Education and scientific Research and Ministry of Electricity for sponsoring this Work.

REFERENCES

[1] A. Faghri, ‘‘Heat pipe science and technology,’’ Global Digital Press, 2015.
[2] D. R. Reay, McGlen, and P. Kew, ‘‘Heat pipes: Theory, design and applications,’’ Butterworth-Heinemann, 2014.
[3] G. P. Peterson, ‘‘An Introduction to Heat Pipes Modelling, Testing, and Applications’’, John Wiley & Sons, Inc., 1994.
[4] S. H. Noie, “Heat transfer characteristics of a two-phase closed thermosiphon,” Appl. Therm. Eng., vol. 25, no. 4, pp. 495–506, 2005.
[5] B. Jiao et al, “Investigation on the effect of filling ratio on the steady-state heat transfer performance of a vertical two-phase closed thermosiphon,” Appl. Therm. Eng., vol. 28, no. 11–12, pp. 1417–1426, 2008.
[6] H. Jouhara and A. J. Robinson, “Experimental investigation of small diameter two-phase closed thermosiphons charged with water, FC-84, FC-77 and FC-3283,” Appl. Therm. Eng., vol. 30, no. 2–3, pp. 201–211, 2010.
[7] A. K. Mozumder et al, “Performance of Heat Pipe for Different working fluids and fill ratios,” J. Mech. Eng., vol. 41, no. 2, pp. 96–102, 2010.
[8] T. Sukchana and C. Jaiboonma, “Effect of Filling Ratios and Adiabatic Length on Thermal Efficiency of Long Heat Pipe Filled with R-134a,” Energy Procedia, vol. 34, pp. 298–306, 2013.
[9] A. A. Chehade et al, and N. Abouzahab-Damaj, “Experimental investigation of thermosiphon loop thermal performance,” Energy Convers. Manag., vol. 84, pp. 671–680, 2014.

[10] R. Manimaran et al, “An Investigation of Thermal Performance of Heat Pipe Using Di-water,” Sci. Technol., vol. 2, no. 4, pp. 77–80, 2012.
[11] E. Sadeghinezhad et al, “Experimental investigation of the effect of graphene nanofluids on heat pipe thermal performance,” Appl. Therm. Eng., vol. 100, pp. 775–787, 2016.
[12] M. Ghanbarpour et al, “Thermal performance of inclined screen mesh heat pipes using silver nanofluids,” Int. Commun. Heat Mass Transf., vol. 67, pp. 14–20, 2015.
[13] Z. Xue and W. Qu, “Experimental study on effect of inclination angles to ammonia pulsating heat pipe,” Chinese J. Aeronaut., vol. 27, no. 5, pp. 1122–1127, 2014.
[14] R. Senthilkumar et al, “Effect of inclination angle in heat pipe performance using copper nanofluid,” Procedia Eng., vol. 38, pp. 3715–3721, 2012.
[15] M. Nazarimanesh et al, “Experimental study on the effects of inclination situation of the sintered heat pipe on its thermal performance,” Exp. Therm. Fluid Sci., vol. 68, pp. 625–633, 2015.
[16] B. Fadhl et al, “Numerical modelling of the temperature distribution in a two-phase closed thermosiphon,” Appl. Therm. Eng., vol. 60, no. 1–2, pp. 122–131, 2013.
[17] A. Alizadehdakhel et al, “CFD modelling of flow and heat transfer in a thermosiphon,” Int. Commun. Heat Mass Transf., vol. 37, no. 3, pp. 312–318, 2010.
[18] G. Huminic and A. Huminic, “Numerical study on heat transfer characteristics of thermosyphon heat pipes using nanofluids,” Energy Convers. Manag., vol. 76, pp. 393–399, 2013.
[19] B. Fadhl et al, “CFD modelling of a two-phase closed thermosiphon charged with R134a and R404a,” Appl. Therm. Eng., vol. 78, pp. 482–490, 2015.
[20] B. Abdullahi, “Development and Optimization of heat pipe based Compound Parabolic Collector,” Thesis submitted to University of Birmingham, 2015.
[21] Y. Kim et al, “Effects of mass transfer time relaxation parameters on condensation in a thermosyphon,” J. Mech. Sci. Technol., vol. 29, no. 12, pp. 5497–5505, 2015.
[22] S. C. K. De Schepper, G. J. Heynderickx, and G. B. Marin, “Modeling the evaporation of a hydrocarbon feedstock in the convection section of a steam cracker,” Comput. Chem. Eng., vol. 33, no. 1, pp. 122–132, 2009.
[23] Z. Yang et al, “Numerical and experimental investigation of two phase flow during boiling in a coiled tube,” Int. J. Heat Mass Transf., vol. 51, no. 5–6, pp. 1003–1016, 2008.
[24] C. Fang et al, “Volume of Fluid Simulation of Boiling Two-Phase Flow in a Vapour-Venting Microchannel,” Front. Heat Mass Transf., vol. 1, no. 1, 2010.
[25] S. C. K. De Schepper et al, “CFD modelling of all gas-liquid and vapour-liquid flow regimes predicted by the Baker chart,” Chem. Eng. J., vol. 138, no. 1–3, pp. 349– 357, 2008.
[26] H. Ganapathy et al, “Volume of fluid-based numerical modeling of condensation heat transfer and fluid flow characteristics in microchannels,” Int. J. Heat Mass Transf., vol. 65, pp. 62–72, 2013.
[27] S. Ghorai and K. D. P. Nigam, “CFD modeling of flow profiles and interfacial phenomena in two-phase flow in pipes,” Chem. Eng. Process. Process Intensif., vol. 45, no. 1, pp. 55–65, 2006.
[28] ANSYS FLUENT, Theory Guide (Release 15.0). ‘‘Multiphase Flows,’’ ANSYS, Inc., November 2013, pp. 465-600 (chapter 17).
[29] J. Brackbill, D. Kothe, and C. Zemach, “A continuum method for modelling surface tension,” J. Comput. Phys., vol. 100, pp. 335–354, 1992.
[30] ANSYS FLUENT, User’s Guide (Release 15.0). ‘‘Modelling Multiphase Flows,’’ ANSYS, Inc., November 2013, pp. 1243-1387 (chapter 25).
[31] R. Ahmadi and T. Okawa, “Influence of surface wettability on bubble behaviour and void evolution in subcooled flow boiling,” International Journal of Thermal Sciences., vol. 97, pp. 114–125, 2015.